The effect of Local Thermal Non-Equilibrium on forced convection boundary layer flow from a heated surface in porous media

M. Celli[a] ; D.A.S. Rees[b] ; A. Barletta[a]

[a] *Dipartimento di Ingegneria Energetica, Nucleare e del Controllo Ambientale (DIENCA), Università di Bologna, Via dei Colli 16, I–40136 Bologna, Italy*

[b] *Department of Mechanical Engineering, University of Bath, Bath, BA2 7AY, UK*

michele.celli3@unibo.it

D.A.S.Rees@bath.ac.uk

antonio.barletta@unibo.it

Abstract

A steady two-dimensional forced convective thermal boundary layer flow in a porous medium is studied. It is assumed that the solid matrix and fluid phase which comprise the porous medium are subject to local thermal non-equilibrium conditions, and therefore two heat transport equations are adopted, one for each phase. When the basic flow velocity is sufficiently high, the thermal fields may be described accurately using the boundary layer approximation, and the resulting parabolic system is analysed both analytically and numerically. Local thermal non-equilibrium effects are found to be at their strongest near the leading edge, but these decrease with distance from the leading edge and Local Thermal Equilibrium is attained at large distances.

Keywords — Laminar flow; Forced convection; Darcy model; Parabolic equation; Porous medium; Local thermal non-equilibrium; Thermal boundary layer.

Nomenclature

c	specific heat at constant pressure
C_1, C_2	constants
h	inter-phase heat transfer coefficient
H	scaled value of h
k	thermal conductivity
K	permeability
p	pressure
T	temperature
T_w	surface temperature
T_∞	temperature outside the boundary layer
U_∞	base flow velocity
u, v	velocity components
x, y	Cartesian coordinates

Greek symbols

α	effective thermal diffusivity
ϕ, Φ	nondimensional solid temperature, Eq. (7)
φ	porosity
γ	nondimensional parameter, Eq. (10)
η	boundary layer variable, Eq. (17)
Λ	threshold parameter, Eq. (56)
μ	dynamic viscosity
θ, Θ	nondimensional fluid temperature, Eq. (7)
ρ	mass density
ξ	streamwise boundary layer variable, Eq. (17)

Superscript, subscripts

	dimensional quantity
˜	nondimensional quantity
f	fluid phase
s	solid phase
∞	ambient conditions

1 Introduction

Heat transfer in porous media arises in a very large number of important applications and it is usually assumed that the temperature fields of the solid and fluid phases are identical locally; such a situation is generally known as Local Thermal Equilibrium (LTE). The opposite situation is known as Local Thermal Non-Equilibrium (LTNE), and in these cases the solid matrix may have a different temperature from that of the saturating fluid, this being meant in terms of averages over representative elementary volumes. Thus, hot fluid may flow into a cold, relatively insulating, porous matrix and there will exist a difference in the average local temperature of the two phases. This difference will take time to reduce to values such that the phases are in LTE (see [1], for example), although there are configurations for which LTNE persists even in the steady state (e.g. [2] and [3]). When the phases are not in LTE the usual single heat transport equation is replaced by a pair of equations, one for each phase. First introduced by Anzelius [4] and Schumann [5], these equations use simple linear source/sink terms to model the local (i.e. microscopic) heat transfer between the phases at the pore level. These early equations have been used in several subsequent studies, especially for the modeling of heat exchangers. The standard equations that are now used routinely are those quoted by Nield and Bejan [6]. The review by Kuznetsov [7] concentrates on forced convection phenomena in the presence of LTNE, while the slightly more recent review by Rees and Pop [8] summarises much of the present knowledge of free and mixed convection and stability analyses.

In the present work a steady forced convection thermal boundary layer flow in a porous medium is studied. This configuration bears a great deal of similarity to the classical Pohlhausen problem in that a thermal boundary layer is induced by a step change in the temperature of a semi-infinite flat plate [9]. The only difference is that here we are dealing with saturated porous media and not with clear fluids. The study of thermally developing forced convection in porous media is also treated in recent papers by Nield *et al.* [10] - [12]. Here it is assumed that the two phases, solid and fluid, are not in local thermal equilibrium and therefore two heat transport equations are adopted. Conditions are determined within which the boundary layer approximation may be made and we undertake an analytical and numerical study of the resulting temperature fields. After a suitable rescaling, the resulting equations are found to depend on just one parameter, γ, which, in turn, is defined in terms of the porosity of the medium and the thermal conductivities of the two phases. The resulting thermal boundary layer equations are then solved in three different ways: (i) analytically by means of a small-x asymptotic analysis, (ii) analytically using a large-x series solution and (iii) numerically by means of a Keller box code. The small-x analysis requires the use of two asymptotic regions, one of which is narrow and is such that the temperature of the fluid phase drops to the ambient value at leading order, and a second much thicker region

within which the temperature of the solid phase drops to the ambient. Asymptotic matching between these two regions is performed and described briefly. This analysis is guided by the earlier study of Rees and Pop [2] who considered the effect of LTNE on a vertical free convective boundary layer flow. The two-layer structure is then modeled numerically by using the results of the asymptotic analysis to devise a modified outer boundary condition for the solid temperature. The numerical solution is further facilitated by the use of properly rescaled variables.

Local thermal non-equilibrium between the solid matrix and the fluid phase is found to be at its strongest near the leading edge, but the maximum difference between the temperatures of the phases decreases with distance from the leading edge, and Local Thermal Equilibrium is attained at large distances.

2 Mathematical model

A steady flow in forced convection regime over a horizontal flat plate is assumed. A sketch of the plate and of the coordinate system is shown in Figure 1. The Darcy model for the porous medium is assumed to hold, and therefore the externally-generated fluid motion is both uniform in space and constant in time. The impermeable bounding surface, which is placed at $\overline{y} = 0$, is held at the temperature, T_w, in the range, $\overline{x} > 0$, but is held at the temperature of the free stream, T_∞, in the range, $\overline{x} < 0$. The point, $(\overline{x}, \overline{y}) = (0, 0)$, at which the boundary condition for the temperature changes, will be regarded the as leading edge of the surface.

Given that the solid and fluid phases are not in LTE, separate heat transport equations for the solid and fluid phases are employed. Thus the governing mass, momentum and thermal energy balance equations in the steady state may be expressed in the form,

$$\frac{\partial \overline{u}}{\partial \overline{x}} + \frac{\partial \overline{v}}{\partial \overline{y}} = 0, \tag{1}$$

$$\overline{u} = -\frac{K}{\mu}\frac{\partial \overline{p}}{\partial \overline{x}}, \qquad \overline{v} = -\frac{K}{\mu}\frac{\partial \overline{p}}{\partial \overline{y}}, \tag{2}$$

$$\varphi\alpha_f\left(\frac{\partial^2 \overline{T}_f}{\partial \overline{x}^2} + \frac{\partial^2 \overline{T}_f}{\partial \overline{y}^2}\right) + \frac{h}{(\rho\, c)_f}\left(\overline{T_s} - \overline{T_f}\right) = \overline{u}\frac{\partial \overline{T}_f}{\partial \overline{x}} + \overline{v}\frac{\partial \overline{T}_f}{\partial \overline{y}} \tag{3}$$

$$(1-\varphi)\alpha_s\left(\frac{\partial^2 \overline{T}_s}{\partial \overline{x}^2} + \frac{\partial^2 \overline{T}_s}{\partial \overline{y}^2}\right) + \frac{h}{(\rho\, c)_s}\left(\overline{T_f} - \overline{T_s}\right) = 0. \tag{4}$$

The thermal boundary conditions are given by

$$\begin{aligned} \overline{y} = 0 \ (\overline{x} < 0): \qquad & \overline{T}_s = \overline{T}_f = \overline{T}_\infty \\ \overline{y} = 0 \ (\overline{x} > 0): \qquad & \overline{T}_s = \overline{T}_f = \overline{T}_w, \\ \overline{y} \to \infty: \qquad & \overline{T}_s, \overline{T}_f \to \overline{T}_\infty. \end{aligned} \tag{5}$$

The quantity, h, which appears in Eqs. (3) and (4), is a function of the microscopic geometry of the medium, the conductivities of the phases and the strength of the flow. Some values of h for stagnant two- and three-dimensional media of various types are given in some very recent papers by Rees [13, 14].

2.1 Nondimensionalization

Given that this is a forced convection problem, the velocity field is given by,

$$(\overline{u}, \overline{v}) = (\overline{U}_\infty, 0), \tag{6}$$

and this may be used immediately in Eq. (3).

A semi-infinite domain such as the one described in Figure 1 implies that there is no natural physical lengthscale on which to base a Péclet number and to use for nondimensionalization. However, the quantity, $\alpha_f/\overline{U}_\infty$, has the dimensions of length, and may be used for this purpose. It turns out to be a little more convenient to use $\varphi\alpha_f/\overline{U}_\infty$ as the lengthscale, and therefore let us introduce nondimensional variables using the following scalings,

$$(\overline{x}, \overline{y}) = \frac{\varphi\alpha_f}{\overline{U}_\infty}(\tilde{x}, \tilde{y}), \qquad (\overline{T}_f, \overline{T}_s) = (\overline{T}_w - \overline{T}_\infty)(\theta, \phi) + \overline{T}_\infty. \tag{7}$$

On using Eqs. (3) and (7), Eqs. (3) and (4) become,

$$\frac{\partial^2\theta}{\partial\tilde{x}^2} + \frac{\partial^2\theta}{\partial\tilde{y}^2} + H(\phi - \theta) = \frac{\partial\theta}{\partial\tilde{x}}, \tag{8}$$

$$\frac{\partial^2\phi}{\partial\tilde{x}^2} + \frac{\partial^2\phi}{\partial\tilde{y}^2} + H\gamma(\theta - \phi) = 0, \tag{9}$$

where

$$H = \frac{\varphi h\alpha_f}{\overline{U}_\infty^2(\rho c)_f}, \qquad \gamma = \frac{\varphi\, k_f}{(1-\varphi)\, k_s} = \frac{\varphi\alpha_f(\rho c)_s}{(1-\varphi)\alpha_s(\rho c)_f}. \tag{10}$$

2.2 Boundary layer approximation

The system formed by Eqs. (8) and (9) is elliptic, and therefore, for $O(1)$ values of H, a fully elliptic numerical simulation should be undertaken to obtain the resulting temperature fields of the two phases. The forced convection regime assumed implies that a high velocity basic

flow is taken into account so that the limit $\overline{U}_\infty \gg 1$ is considered. From the definition of H in Eq. (10), $\overline{U}_\infty \gg 1$ implies that $H \ll 1$. Assuming now that $H \ll 1$, it is necessary to balance the magnitudes of the last three terms in Eq. (8), and it may be shown easily that the appropriate orders of magnitude are $\tilde{x} = O(H^{-1})$ and $\tilde{y} = O(H^{-1/2})$. Therefore the scalings,

$$\tilde{x} = H^{-1}x, \qquad \tilde{y} = H^{-1/2}y, \tag{11}$$

are introduced into Eqs. (8) and (9) to obtain,

$$H\frac{\partial^2\theta}{\partial x^2} + \frac{\partial^2\theta}{\partial y^2} + (\phi - \theta) = \frac{\partial\theta}{\partial x}, \tag{12}$$

$$H\frac{\partial^2\phi}{\partial x^2} + \frac{\partial^2\phi}{\partial y^2} + \gamma(\theta - \phi) = 0. \tag{13}$$

Formally allowing $H \to 0$ yields the boundary layer approximation naturally, and the governing equations are now,

$$\frac{\partial\theta}{\partial x} = \frac{\partial^2\theta}{\partial y^2} + (\phi - \theta), \tag{14}$$

$$\frac{\partial^2\phi}{\partial y^2} + \gamma\,(\theta - \phi) = 0. \tag{15}$$

This system of equations is parabolic, and although it may be shown that there does not exist a self-similar solution, there is nevertheless a nonsimilar formulation which may be found; this analysis follows below.

2.3 Boundary layer transformation

It is well-known that the equation formed by the first two terms of Eq. (14) admits the self-similar solution,

$$\theta = \operatorname{erfc}\left(\frac{y}{2\sqrt{x}}\right), \tag{16}$$

The solution shown in Eq.(16) can be found, for instance, in Özişik [15], and it motivates the following coordinate transformations,

$$\eta = \frac{y}{2\sqrt{x}}, \quad \xi = \sqrt{x}, \qquad \theta = \Theta(\xi,\eta), \quad \phi = \Phi(\xi,\eta), \tag{17}$$

where the upper case characters, Θ and Φ, will henceforth denote the respective temperatures of the fluid and solid phases in this new coordinate system, while the lower case characters, θ and ϕ, correspond to the solution written in Cartesian coordinates. Eqs. (14) and (15) become

$$\frac{\partial^2 \Theta}{\partial \eta^2} - 2\,\xi\,\frac{\partial \Theta}{\partial \xi} + 2\,\eta\,\frac{\partial \Theta}{\partial \eta} + 4\,\xi^2\,(\Phi - \Theta) = 0, \tag{18}$$

$$\frac{\partial^2 \Phi}{\partial \eta^2} + 4\,\xi^2\,\gamma\,(\Theta - \Phi) = 0, \tag{19}$$

which are to be solved subject to the boundary conditions,

$$\begin{aligned} \eta = 0 \;\text{ and }\; \xi > 0: &\qquad \Theta = \Phi = 1, \\ \eta \to \infty \;\text{ and }\; \xi > 0: &\qquad \Theta,\, \Phi \;\to\; 0. \end{aligned} \tag{20}$$

It is important to note that the coefficient, ξ^2, of the source/sink terms in Eqs. (18) and (19) plays the same role as H does in Eqs. (8) and (9). Therefore it is possible to observe immediately that large values of ξ will correspond to Local Thermal Equilibrium, while Local Thermal Non-Equilibrium effects will be at their strongest near the leading edge, $\xi = 0$. These equations have only one nondimensional parameter, namely γ.

3 Asymptotic analyses

The numerical solution of Eqs. (18) and (19) will be preceded by asymptotic analyses close to and far from the leading edge at $\xi = 0$. The near-leading-edge analysis is performed first because it provides the boundary conditions that are essential for the numerical solution.

3.1 Close to the leading edge

The system formed by Eqs. (18) and (19) may be solved in the region relatively close to the leading edge by searching for a solution in the form of a power series in the variable ξ,

$$\begin{aligned} \Theta(\xi,\eta) &= \Theta_0(\eta) + \xi\Theta_1(\eta) + \xi^2\Theta_2(\eta) + \cdots, \\ \Phi(\xi,\eta)) &= \Phi_0(\eta) + \xi\Phi_1(\eta) + \xi^2\Phi_2(\eta) + \cdots. \end{aligned} \tag{21}$$

At leading order in the expansion, the equations for Θ_0 and Φ_0 are,

$$\Theta_0'' + 2\,\eta\,\Theta_0' = 0, \quad \Phi_0'' = 0 \tag{22}$$

and their solutions are

$$\Theta_0 = \operatorname{erfc}(\eta), \quad \Phi_0 = 1. \tag{23}$$

In writing down the above expression for Φ_0, it is important to note that it is impossible to solve $\Phi_0'' = 0$ subject to both $\Phi_0(0) = 1$ and $\Phi_0 \to 0$ as $\eta \to \infty$. The boundary condition

at the heated surface was employed, the implication being that the temperature of the solid phase near the leading edge must then vary over a lengthscale which is much greater than that represented by $O(1)$ values of η. This is consistent with a previous analysis in [2]. It is also clear that Eq. (15) provides a means of satisfying the far field boundary condition; in this regime where $y = O(1)$ the leading order temperature of the fluid phase, Θ_0, has already decayed to zero, leaving a system which admits an exponentially decaying solution. Therefore it is natural to attempt a corresponding solution in this 'outer' region where $y = O(1)$ (noting that the 'inner' region where $\eta = O(1)$ corresponds to $y = O(x^{1/2}) = O(\xi)$). Thus an outer solution of the form,

$$\begin{aligned} \theta(x,y) &\sim \theta_0(y) + \sqrt{x}\theta_1(y) + x\theta_2(y) + \cdots, \\ \phi(x,y) &\sim \phi_0(y) + \sqrt{x}\phi_1(y) + x\phi_2(y) + \cdots, \end{aligned} \tag{24}$$

is sought.

On taking $\theta_0 = 0$ because of the superexponential decay of Θ_0 in the inner region, the leading order equations in the outer region are,

$$\theta_2 = \phi_0, \qquad \phi_0'' - \gamma\,\phi_0 = 0. \tag{25}$$

Given that $\Phi_0 = 1$, the appropriate matching condition for ϕ_0 is that $\phi_0(0) = 1$. Hence ϕ_0 and θ_2 are given by,

$$\theta_2 = \phi_0 = e^{-\sqrt{\gamma}\,y}, \tag{26}$$

which shows that the leading order terms of both temperature fields decay exponentially; this has important implications later for the numerical solutions.

These solutions now provide us with the appropriate matching conditions for the inner solutions at the next order in ξ. On expanding the solutions given in Eq. (26) about $y = 0$ one obtains,

$$\theta \sim (1 - \sqrt{\gamma}\,y + \frac{\gamma\,y^2}{2} + \cdots)\,x, \tag{27}$$

$$\phi \sim 1 - \sqrt{\gamma}\,y + \frac{\gamma\,y^2}{2} + \cdots, \tag{28}$$

and if y is replaced by $2\eta\,\xi$ then the large-η matching conditions for small values of ξ are found to be,

$$\Theta \sim \xi^2 - 2\,\sqrt{\gamma}\,\eta\,\xi^3 + \cdots, \qquad \Phi \sim 1 - 2\,\sqrt{\gamma}\,\eta\,\xi + 2\,\gamma\,\eta^2\,\xi^2 + \cdots. \tag{29}$$

Therefore the following conditions as $\eta \to \infty$ may be written,

$$\Phi_1 \sim -2\sqrt{\gamma}\,\eta, \qquad \Phi_2 \sim 2\gamma\,\eta^2, \qquad \Theta_2 \sim 1. \tag{30}$$

The next terms in the inner region arise at $O(\xi)$. From the expansion at this order one obtains the system

$$\Theta_1'' + 2\,\eta\,\Theta_1' - 2\,\Theta_1 = 0, \quad \Phi_1'' = 0. \tag{31}$$

which is to be solved subject to the conditions,

$$\begin{aligned} \eta = 0: &\qquad \Theta_1 = 0, \quad \Phi_1 = 0, \\ \eta \to \infty: &\qquad \Theta_1 \to 0, \quad \Phi_1 \sim -2\sqrt{\gamma}\,\eta. \end{aligned} \tag{32}$$

The solutions are

$$\Theta_1 = 0, \qquad \Phi_1 = -2\sqrt{\gamma}\,\eta. \tag{33}$$

The solution for ϕ_1 is clearly passive, and it is caused by the leading order exponential properties of ϕ_0.

At $O(\sqrt{x})$ in the outer region, the governing equations are

$$\theta_1'' + \phi_1 - \theta_1 - 2\,\theta_3 = 0, \qquad \phi_1'' + \gamma(\theta_1 - \phi_1) = 0, \tag{34}$$

which are to be solved subject to

$$y = 0: \quad \theta_1 = \phi_1 = 0, \qquad y \to \infty: \quad \theta_1, \phi_1 \to 0. \tag{35}$$

Given that these equations are homogeneous, the solutions are

$$\theta_1 = 0, \quad \theta_3 = 0, \quad \phi_1 = 0. \tag{36}$$

At $O(\xi^2)$ in the inner region, the governing equations are,

$$\Theta_2'' - 4\,\Theta_2 + 2\,\eta\,\Theta_2' + 4\,\mathrm{erf}(\eta) = 0, \quad \Phi_2'' - 4\,\gamma\,\mathrm{erf}(\eta) = 0, \tag{37}$$

$$\begin{aligned} \eta = 0: &\quad \Theta_2 = 0, \quad \Phi_2 = 0, \\ \eta \to \infty: &\quad \Theta_2 \to 1, \quad \Phi_2 \sim 2\,\gamma\,\eta^2, \end{aligned} \tag{38}$$

and the solutions are

$$\Theta_2 = \mathrm{erf}(\eta), \quad \Phi_2 = \eta\,\frac{2e^{-\eta^2}\gamma}{\sqrt{\pi}} + \gamma\left(1 + 2\eta^2\right)\mathrm{erf}(\eta). \tag{39}$$

This is a reasonable point at which to stop the expansion for the inner region because three terms have now been obtained for Φ. At $O(x)$ for the outer region one has

$$\theta_2'' + \phi_2 - \theta_2 - 2\,\theta_4 = 0, \quad \phi_2'' + \gamma(\theta_2 - \phi_2) = 0. \tag{40}$$

which are to be solved using Eq. (26) and subject to

$$y = 0: \quad \phi_2 = 0, \qquad y \to \infty: \quad \phi_2 \to 0, \tag{41}$$

the solution for Eq. (40) is

$$\theta_4 = \frac{e^{-y\sqrt{\gamma}}}{4}\left(2\,\gamma - 2 + y\,\sqrt{\gamma}\right), \quad \phi_2 = e^{-y\,\sqrt{\gamma}}\left(\frac{y\,\sqrt{\gamma}}{2}\right). \tag{42}$$

To summarise, the solutions found by the power series expansion for both the inner and the outer regions are:

$$\Theta \sim \operatorname{erfc}(\eta) + \xi^2 \operatorname{erf}(\eta), \quad \Phi \sim 1 - 2\sqrt{\gamma}\xi\,\eta + \left[\eta\,\frac{2\gamma e^{-\eta^2}}{\sqrt{\pi}} + \gamma\left(1 + 2\eta^2\right)\operatorname{erf}(\eta)\right]\xi^2, \tag{43}$$

$$\theta \sim x\,e^{-y\sqrt{\gamma}}, \quad \phi \sim e^{-y\sqrt{\gamma}} + x\left(\frac{y\,\sqrt{\gamma}}{2}\right)e^{-y\,\sqrt{\gamma}}.$$

3.2 Far from the leading edge

The solutions of Eqs. (18)-(19) at large distances from the leading edge are considered now. When $\xi \gg 1$ there are two possible order-of-magnitude balances that may be obtained from Eq. (19). The first suggests that there is an inner layer of width $\eta = O(\xi^{-1})$ within the main boundary layer, for which we assume that $\eta = O(1)$. The second, and more reasonable one on physical grounds, is that $\theta - \phi = O(\xi^{-2})$, and that there is only one asymptotic region. This second balance corresponds to the approach to LTE. Therefore one may investigate the region far from the leading edge by searching for a solution expressed as a power series expansion of the form

$$\begin{aligned} \Theta(\xi,\eta) &\sim \Theta_0(\eta) + \xi^{-1}\Theta_1(\eta) + \xi^{-2}\Theta_2(\eta) + \cdots, \\ \Phi(\xi,\eta) &\sim \Theta_0(\eta) + \xi^{-1}\Theta_1(\eta) + \xi^{-2}\Theta_2(\eta) + \cdots. \end{aligned} \tag{44}$$

The leading order, i.e. $O(1)$, equations are

$$\Theta_0'' + 2\,\eta\,\Theta_0' + 4\,(\Phi_2 - \Theta_2) = 0, \tag{45}$$

$$\Phi_0'' + 4\,\gamma\,(\Theta_2 - \Phi_2) = 0, \tag{46}$$

while the boundary conditions are

$$\begin{aligned} \eta = 0: &\qquad \Theta = \Phi = 1, \\ \eta \to \infty: &\qquad \Theta, \Phi \to 0. \end{aligned} \tag{47}$$

Given the above argument, one may reasonably assume that $\Phi_0 = \Theta_0$. On multiplying Eq. (45) by γ and adding it to Eq. (46), one obtains

$$(1+\gamma)\,\Theta_0'' + 2\,\eta\,\gamma\,\Theta_0' = 0, \tag{48}$$

the solution for which is,

$$\Phi_0 = \Theta_0 = \operatorname{erfc}\left(\eta\sqrt{\frac{\gamma}{1+\gamma}}\right). \tag{49}$$

At $O(\xi^{-1})$ of the expansion the governing equations are,

$$\Theta_1'' + 2\,\Theta_1 + 2\,\eta\,\Theta_1' + 4\,(\Phi_3 - \Theta_3) = 0, \tag{50}$$

$$\Phi_1'' + 4\,\gamma\,(\Theta_3 - \Phi_3) = 0. \tag{51}$$

The terms in Θ_3 and Φ_3 may be eliminated by means of the same process of combination of the equations, and this results in the following equation,

$$(1+\gamma)\,\Theta_1'' + 2\,\eta\,\gamma\,\Theta_1' + 2\,\gamma\,\Theta_1 = 0. \tag{52}$$

Given the above scaling argument that $\Theta - \Phi = O(\xi^{-2})$, it has been assumed that $\Theta_1 = \Phi_1$. Equation (52) has the general solution,

$$\Phi_1 = \Theta_1 = C_1\,e^{-\frac{\gamma}{1+\gamma}\eta^2}\,\operatorname{erfi}\left(\eta\sqrt{\frac{\gamma}{1+\gamma}}\right) + C_2 e^{-\frac{\gamma}{1+\gamma}\eta^2}, \tag{53}$$

where C_1 and C_2 are constants. This solution should satisfy zero boundary conditions for Θ_1 at both $\eta = 0$ and as $\eta \to \infty$. This implies that $C_2 = 0$, but C_1 remains indeterminate. Clearly, then, the function multiplying C_1 in Eq. (53) is an eigensolution of the equation. Although further terms in this expansion will only be expressed in terms of C_1 and any further eigensolutions which might arise, it is possible, nevertheless, to determine precisely the leading order departure from LTNE. If Eq. (49) is substituted into Eqs. (45) and (46), then it is straightforward to show that

$$\Theta_2 - \Phi_2 = \frac{\Phi_0''}{4\,\gamma} = \sqrt{\frac{\gamma}{\pi\,(1+\gamma)^3}}\;\eta\,e^{-\frac{\gamma}{1+\gamma}\eta^2}. \tag{54}$$

Eq. (54) corresponds to an $O(\xi^{-2})$ difference between the temperatures of the phases. It is also worthy of note that the magnitude of this difference decreases as γ increases; the mathematical reason lies in the fact that a large value of γ forces the difference between the temperatures to be small, as seen in Eq. (19).

4 Numerical solutions

The numerical scheme which was used to solve numerically the system of Eqs. (18)-(19) is a standard Keller box method, which is a generic method for time or space marching problems, [16]. Most often, the system is reduced to first order form in η, the resulting equations discretised half way between the grid points in both the η and ξ directions, and it is therefore of second order accuracy. An initial profile is not required, because the system of parabolic partial differential equations reduces to an ordinary differential system at $\xi = 0$, and a suitably written code will be able to solve this system easily. Although the present system of equations is linear, the general methodology uses a multidimensional Newton-Raphson iteration scheme to solve the discretised equations. In our case the corresponding iteration matrix is computed numerically, and a standard block-Thomas algorithm is used to solve the iteration equations. The x variable is treated here as a time-like variable, and the solution is marched downstream.

In the present implementation we have adopted a backward difference method in x in order to maximise numerical stability, and good accuracy is ensured by employing the small steplength, $\delta\xi = 10^{-2}$. In the η-direction, the steplength, $\delta\eta = 10^{-2}$, is taken with $\eta_{\max} = 20$. However, in the above small-ξ analysis we determined that the leading order temperature fields in the outer region decay as $\exp(-y\sqrt{\gamma})$, i.e. as $\exp(-2\eta\xi\sqrt{\gamma})$ from the point of view of the boundary layer. Therefore it is clear that this rate of decay cannot be contained within a finite computational domain when ξ is sufficiently small. However, it is possible to model this rate of decay by adopting a different set of boundary conditions from those given earlier in Eqs. (20). We used the following,

$$\Theta' + 2\xi\sqrt{\gamma}\Theta = 0, \qquad \Phi' + 2\xi\sqrt{\gamma}\Phi = 0, \qquad \text{at } \eta = \eta_{\max}. \tag{55}$$

These conditions were used from $\xi = 0$ until the first value of ξ at which both Θ and Φ are less than 10^{-6}, and thereafter the conditions given in Eqs. (20) were adopted. In this way the full presence of the outer layer is modelled by means of a modified boundary condition.

Figures 2 - 4 show the temperature profiles obtained by the numerical simulations, and are plotted in the (x, y)-coordinates, as defined in Eq. (11). The three frames in Figure 2 are drawn using the same range of values of x and y, but for different values of γ: the upper frame refers to $\gamma = 0.01$, the central frame to $\gamma = 0.1$ and the lower refers to $\gamma = 1$. Dashed

lines refer to the solid phase and solid lines refer to fluid phase. In this figure it is clear that the thickness of the thermal boundary layer at all values of x is strongly dependent on the magnitude of γ. This is consistent with Eq. (49) which shows clearly that the large-x thickness of the boundary layer increases as γ decreases. Likewise, near the leading edge, the thickness of the thermal boundary layer corresponding to the solid phase increases as γ decreases; see Eq. (25). That this should be so is understood by referring to the physical implications of different values of γ. When γ is small, heat is conducted easily away from the heated surface, and only a small amount is imparted to the fluid. On the other hand, when γ is large, heat is transferred easily to the fluid and is therefore advected downstream, which decreases the thickness of the boundary layers. The ease of heat transfer between the phases may also be seen in Figure 7 local thermal equilibrium is attained at much smaller values of x when $\gamma = 1$ than when $\gamma = 0.01$. Figures 3 and 4 show the same information as Figure 2, but for a progressively smaller range of values of y and x. The variation with γ of the boundary layer thickness of the solid phase near the leading edge may be seen clearly, but it is also possible to see that the boundary layer thickness of the fluid phase is independent of γ there. This independence is consistent with Eq. (23). At slightly increased distances from the leading edge the boundary layer thickness of the fluid phase increases rapidly at a rate which is dependent on γ.

Although γ is the sole parameter of the system being studied, Figures 2 to 4 already indicate substantial variations of the resulting temperature fields as the parameter varies. The surface rate of heat transfer is an important quantity, and the manner in which its evolution with ξ varies with γ is shown in Figure 5. All of our previous observations are seen clearly in this Figure, particularly the magnitude of the rate of heat transfer far from the leading edge. Given that we have plotted the η-derivative of the temperatures, the solid phase now has a zero rate of heat transfer at the leading edge, but this varies rapidly as ξ increases, and does so at a γ-dependent rate. However, of most interest is the distance at which one might say that Local Thermal Equilibrium has been attained. Such a criterion is necessarily arbitrary; we can define x_{LTE} to be the distance beyond which the relative difference of the surface rates of heat transfer, Λ, is less than 1%, namely, that

$$\Lambda = 2\left(\left.\frac{\partial\theta}{\partial y}\right|_{y=0} - \left.\frac{\partial\phi}{\partial y}\right|_{y=0}\right) \Big/ \left(\left.\frac{\partial\theta}{\partial y}\right|_{y=0} + \left.\frac{\partial\phi}{\partial y}\right|_{y=0}\right) \leq 0.01. \tag{56}$$

The behaviour of the parameter Λ as a function of x is shown in Figure 6. This figure confirms the results previously obtained in Figure 5 for which as γ increases the heat transfer between the two phases decreases more quickly. Thus also the distance from the leading edge x_{LTE} defined by Eq.(56) decreases as γ increases. This behaviour is displayed in Figure 7 and the relative Table 1. The value of x_{LTE}, in fact, decreases monotonically as γ increases.

5 Conclusion

A steady two−dimensional forced convection thermal boundary layer in a porous medium has been studied both analytically and numerically. The main focus has been on the effect of local thermal non−equilibrium between the solid and fluid phases. Separate asymptotic analyses which are valid at small distances and at large distances from the leading edge have been obtained. In particular, we have determined that the boundary layer in the near-leading-edge region splits into two well-defined asymptotic regions, one in which y is the natural variable, and the other in which η is the natural variable. This analysis was used to obtain an effective outer boundary condition for the numerical study which would take into account accurately the presence of the outer region. The large-ξ asymptotic analysis shows that local thermal equilibrium is attained in this limit, with local thermal non-equilibrium effects being of $O(x^{-1})$ in magnitude. A full numerical solution was also obtained and solutions presented. We found that:

- the thickness of the boundary layers of each phase depends strongly on the value of γ;
- the thickness of fluid boundary layer near the leading edge is independent of γ;
- the boundary layer corresponding to the solid phase is always thicker than that of the fluid phase;
- local thermal equilibrium is attained at decreasing distances from the leading edge as γ increases; this is related to the increasing ease of heat transfer between the phases.

Finally, it is important to note that the flows we have considered may be subject to thermoconvective instability. Papers by Rees and Bassom [17] and Rees [18]–[20] are concerned with various aspects of the instability of free convection boundary layers, while Rees [21] is concerned with linear instability and the nonlinear vortex development in a mixed convection flow where forced convection effects are strong compared with buoyancy. The situation described in [21] could be applied to the flow considered here if weak buoyancy forces are allowed to exist. As the flow develops downstream, the local Rayleigh number, which is proportional to the boundary layer thickness, also increases and eventually becomes sufficiently large that thermoconvective instability will occur. It is intended to report on this aspect elsewhere.

References

[1] D.A.S. Rees, A.P. Bassom, P.G. Siddheshwar, Local thermal non-equilibrium effects arising from the injection of a hot fluid into a cold porous medium. *J. Fluid Mechanics*, **594**, pp. 379–398, (2007).

[2] D.A.S. Rees, I.Pop, Vertical free convective boundary-layer flow in a porous medium using a thermal nonequilibrium model. *J. Porous Media*, **3**, pp. 31–44, (2000).

[3] D.A.S. Rees, Vertical free convective boundary-layer flow in a porous medium using a thermal nonequilibrium model: elliptical effects. *J. Appl. Math. Phys. (ZAMP)*, **54**, pp. 437–448 (2003).

[4] A. Anzelius, Über Erwärmung vermittels durchströmender. *Medien. Zeit. Ang. Math. Mech.*, **6**, pp. 291-294, (1926).

[5] T.E.W. Schumann, Heat transfer: liquid flowing through a porous prism. *Journal of the Franklin Institute*, **208**, pp. 405-416, (1929).

[6] D.A. Nield, A. Bejan, *Convection in Porous Media* (3rd edition). Springer, New York, (2006).

[7] A.V. Kuznetsov, Thermal nonequilibrium forced convection in porous media. *Transport Phenomena in Porous Media (*eds. *D.B.Ingham and I.Pop)*, Pergamon, pp. 103-129, (1998).

[8] D.A.S. Rees, I. Pop, Local thermal nonequilibrium in porous medium convection. *Transport Phenomena in Porous Media III (*eds. *D.B.Ingham and I.Pop)*, Pergamon, pp. 147-173, (2005).

[9] K. Pohlhausen, Der Wärmeaustausch zwischen festen Körpen und Flüssigkeiten mit kleiner Reibung und kleiner Wärmeleitung. *Z. Angew. Math. Mech.* **1**, pp. 115-124, (1921).

[10] D.A. Nield, A.V. Kuznetsov, M. Xiong, Effect of local thermal non-equilibrium on thermally developing forced convection in a porous medium. *Int. J. Heat Mass Transfer*, **45**, pp. 4949-4955, (2002).

[11] A.V. Kuznetsov, D.A. Nield, Thermally developing forced convection in a bidisperse porous medium. *J. Porous Media*, **9**, pp. 393-402, (2006).

[12] A.V. Kuznetsov, D.A. Nield, Thermally developing forced convection in a porous medium occupied by a rarefied gas: parallel plate channel or circular tube with walls at constant heat flux. *Transp. Porous Media*, **76**, pp. 345-362, (2009).

[13] D.A.S. Rees, Microscopic modelling of the two-temperature model for conduction in heterogeneous media. *J. of Porous Media* **13**, pp. 125-143, (2010).

[14] D.A.S. Rees, Microscopic modelling of the two-temperature model for conduction in heterogeneous media: three-dimensional media. *Proceedings of the 4th International Conference on Applications of Porous Media, Istanbul, Turkey* Paper 15, (August 2009).

[15] M.N. Özişik, Heat conduction. *Wiley, John and Sons* **2nd edition**, (1993).

[16] H.B. Keller, T. Cebeci, Accurate numerical methods for boundary layer flows 1. Two dimensional Flows. *Proc. Int. Conf. Numerical Methods in Fluid Dynamics, Lecture Notes in Physics, Springer - New York* (1971),

[17] D.A.S. Rees, A.P. Bassom, The nonlinear nonparallel wave instability of free convection induced by a horizontal heated surface in fluid-saturated porous media. *J. Fluid Mechanics* **253**, pp. 267-296, (1993),

[18] D.A.S. Rees, Vortex instability from a near-vertical heated surface in a porous medium. I Linear theory. *Proc. Roy. Soc.* **A457**, pp. 1721-1734, (2001).

[19] D.A.S. Rees, Vortex instability from a near-vertical heated surface in a porous medium. II Nonlinear evolution. *Proc. Roy. Soc.* **A458**, pp. 1575–1592, (2002).

[20] D.A.S. Rees, Nonlinear vortex development in free convective boundary layers in porous media. *NATO ASI proceedings, Neptun, Romania, June 9-20 2003*, pp. 449-458, (2003).

[21] D.A.S. Rees, The onset and nonlinear development of vortex instabilities in a horizontal forced convection boundary layer with uniform surface suction. *Transport in Porous Media* **77**, pp. 243–265, (2009).

Figure captions

Figure 1 — A geometrical sketch of the problem.

Figure 2 — Isotherms for both the solid and fluid phases for $\gamma = 0.01$ (upper), $\gamma = 0.1$ (middle), $\gamma = 1$ (lower). Dashed lines refer to the solid phase and solid lines refer to fluid phase.

Figure 3 — Isotherms for both the solid and fluid phases for $\gamma = 0.01$ (upper), $\gamma = 0.1$ (middle), $\gamma = 1$ (lower). Dashed lines refer to the solid phase and solid lines refer to fluid phase. This Figure has a different vertical resolution to that shown in Figure 2.

Figure 4 — Isotherms for both the solid and fluid phases for $\gamma = 0.01$ (upper), $\gamma = 0.1$ (middle), $\gamma = 1$ (lower). Dashed lines refer to the solid phase and solid lines refer to fluid phase. This Figure has a different vertical resolution to that shown in Figure. 2.

Figure 5 — Variation of the rates of heat transfer, $\partial\theta/\partial\eta$ and $\partial\phi/\partial\eta$, on the plate $\eta = 0$ versus ξ, for different values of γ. Dashed lines refer to the solid phase and solid lines to the fluid phase.

Figure 6 — Behaviour of the parameter Λ as a function of x for different values of γ.

Figure 7 — Variation with γ of the distance, x_{LTE}, at which local thermal equilibrium is attained.

γ	x_{LTE}
0.01	10.011
0.02	9.8345
0.05	9.4618
0.1	9.0000
0.2	8.2484
0.5	6.7808
1	5.4289
2	4.0280
5	2.5027
10	1.6770
20	1.0858
50	0.6053
100	0.3856
200	0.2450
500	0.1332
1000	0.0841

Table 1: Variation with γ of the distance, x_{LTE}, at which local thermal equilibrium is attained. Threshold for the achieving of LTE is chosen to be when the parameter $\Lambda \leq 0.01$.

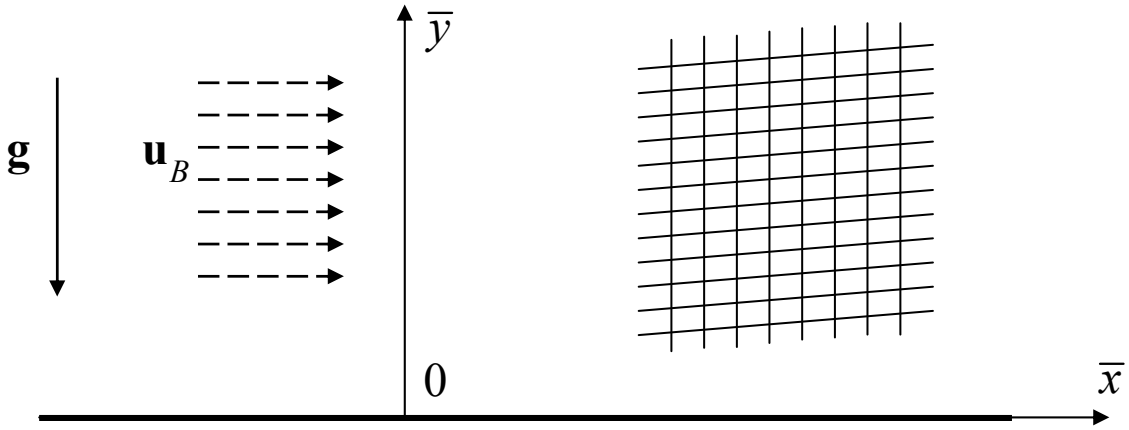

Figure 1: A geometrical sketch of the problem

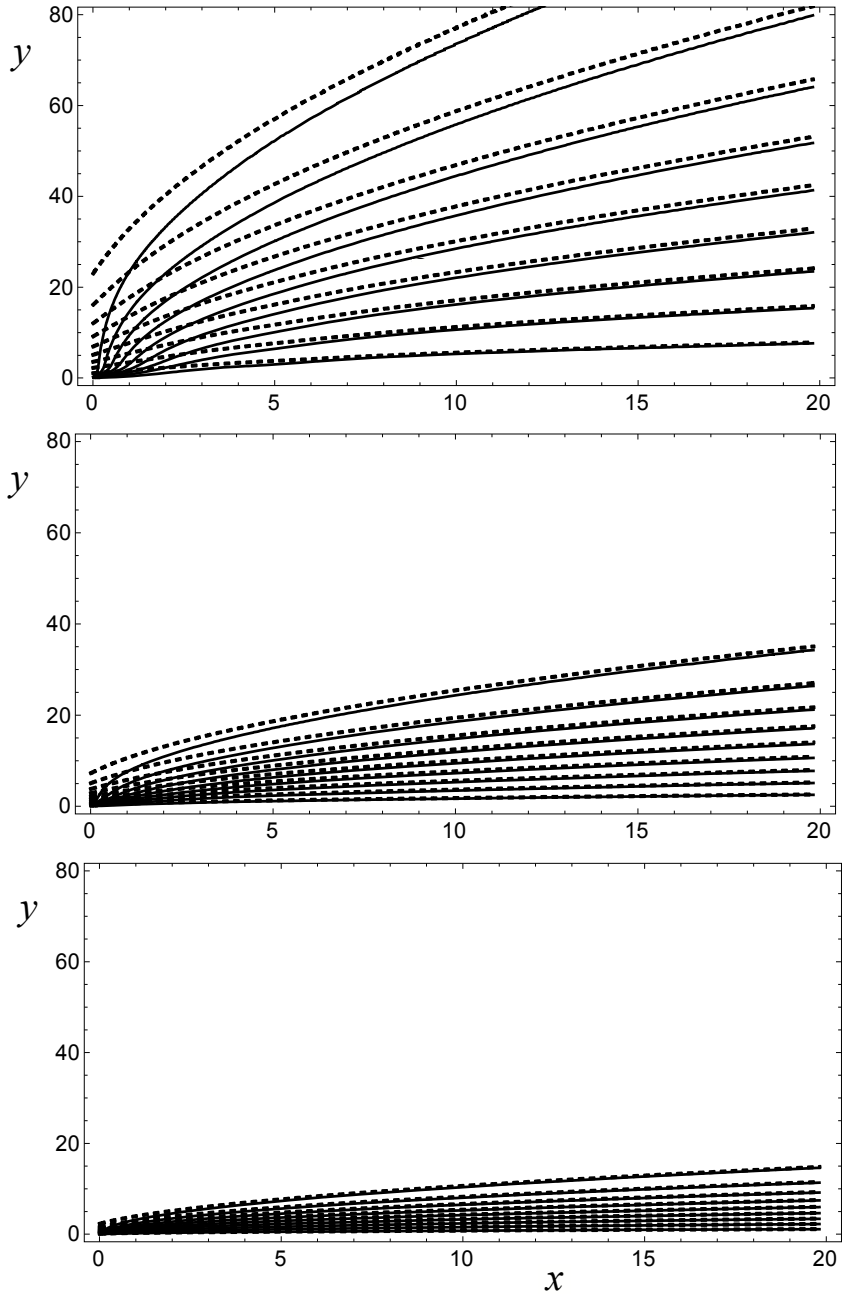

Figure 2: Isotherms for both the solid and fluid phases for $\gamma = 0.01$ (upper), $\gamma = 0.1$ (middle), $\gamma = 1$ (lower). Dashed lines refer to the solid phase and solid lines refer to fluid phase.

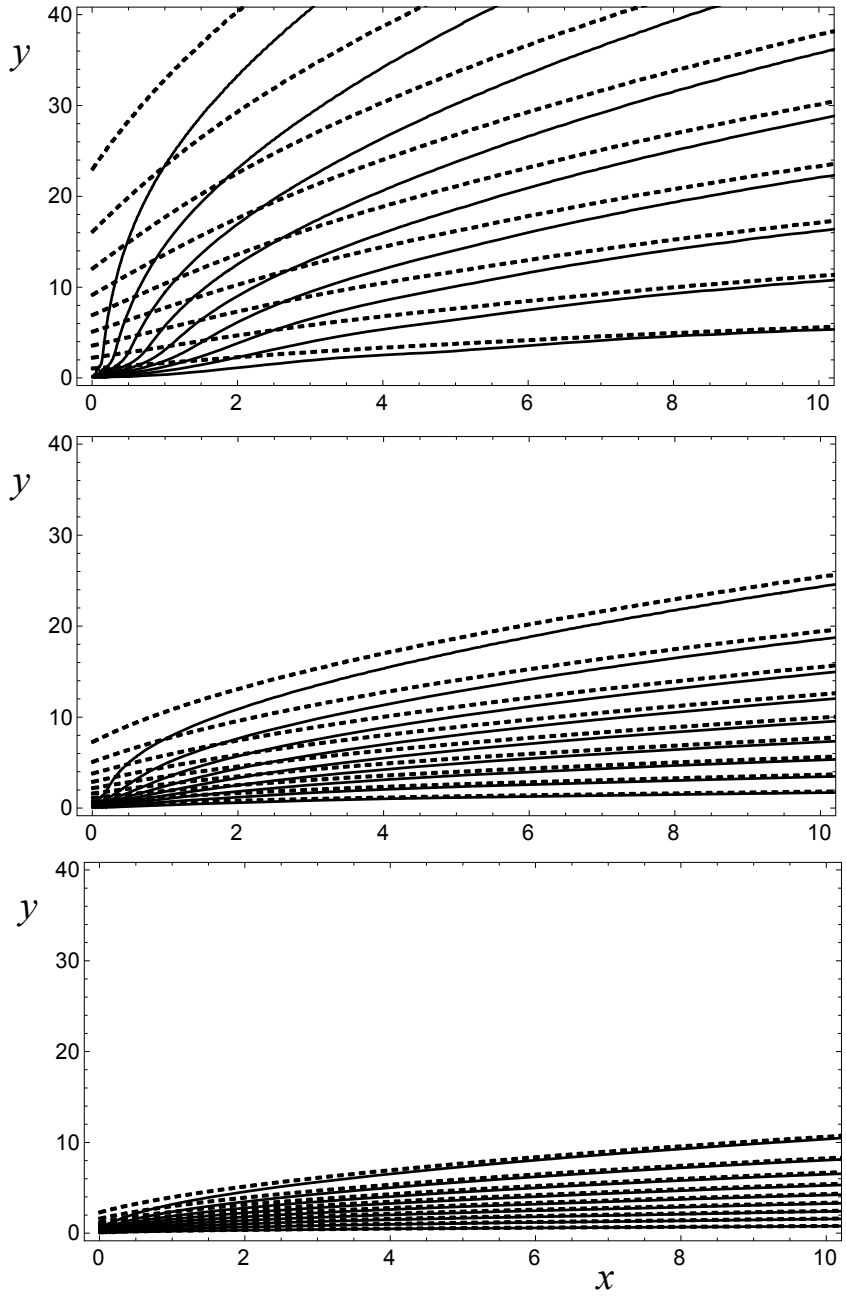

Figure 3: Isotherms for both the solid and fluid phases for $\gamma = 0.01$ (upper), $\gamma = 0.1$ (middle), $\gamma = 1$ (lower). Dashed lines refer to the solid phase and solid lines refer to fluid phase. This Figure has a different vertical resolution to that shown in Figure 2.

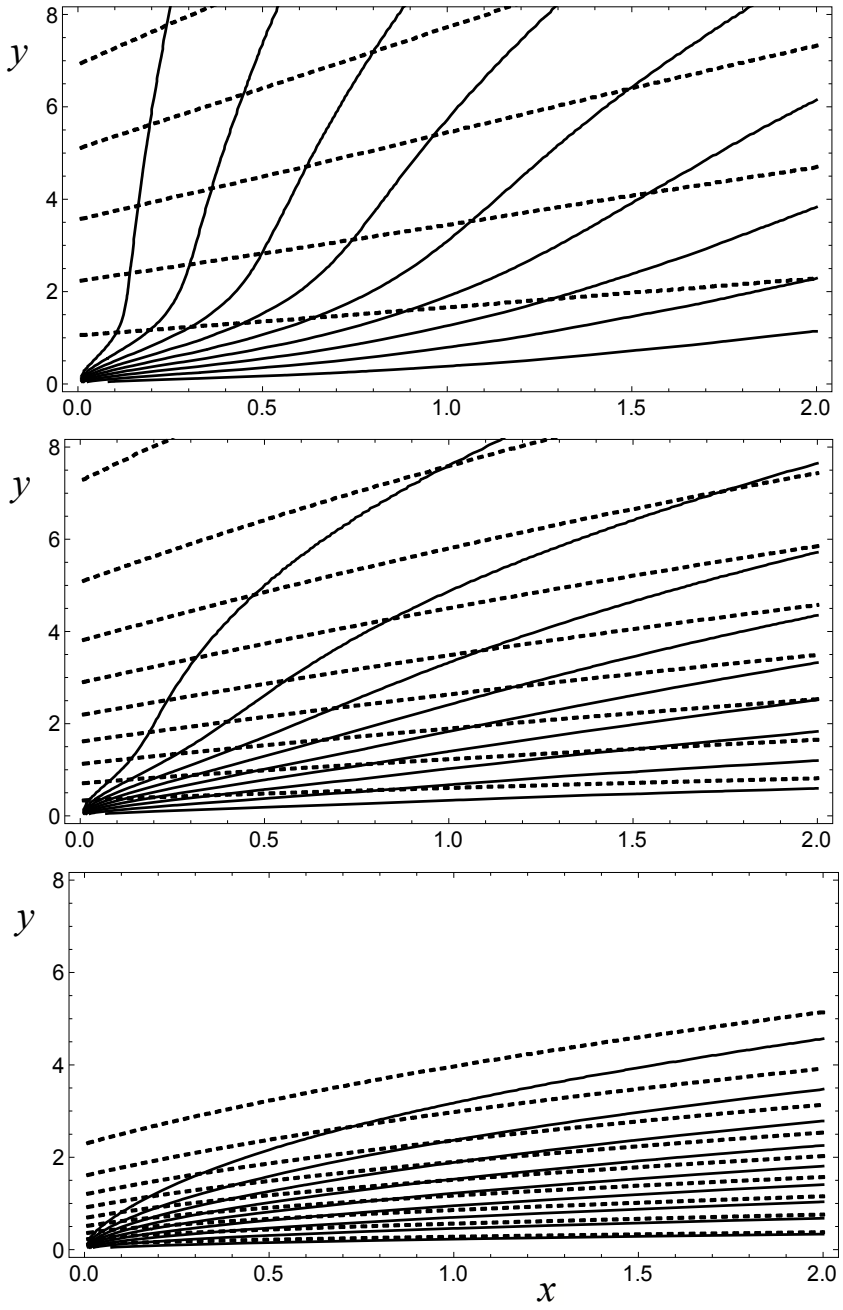

Figure 4: Isotherms for both the solid and fluid phases for $\gamma = 0.01$ (upper), $\gamma = 0.1$ (middle), $\gamma = 1$ (lower). Dashed lines refer to the solid phase and solid lines refer to fluid phase. This Figure has a different vertical resolution to that shown in Figure 2.

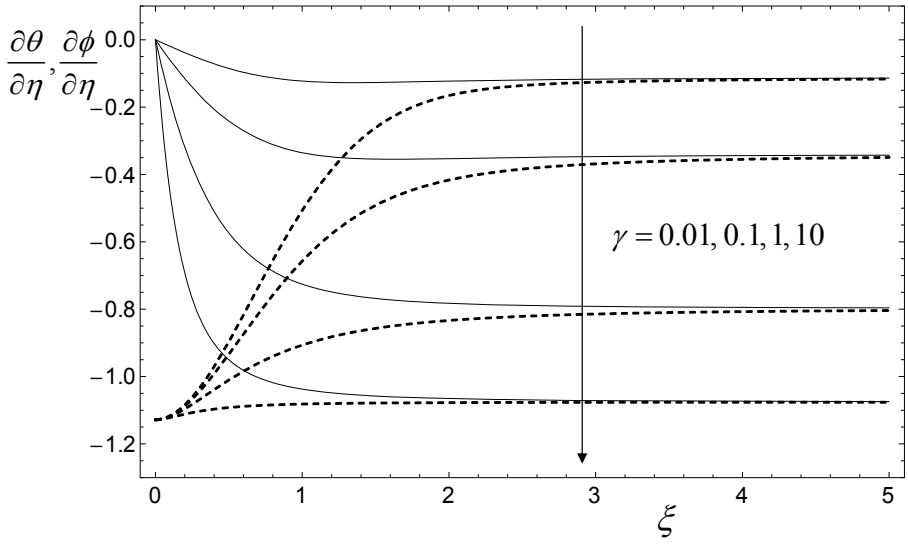

Figure 5: Variation of the rates of heat transfer, $\partial\theta/\partial\eta$ and $\partial\phi/\partial\eta$, on the plate $\eta = 0$ versus ξ, for different values of γ. Dashed lines refer to the solid phase and solid lines to the fluid phase.

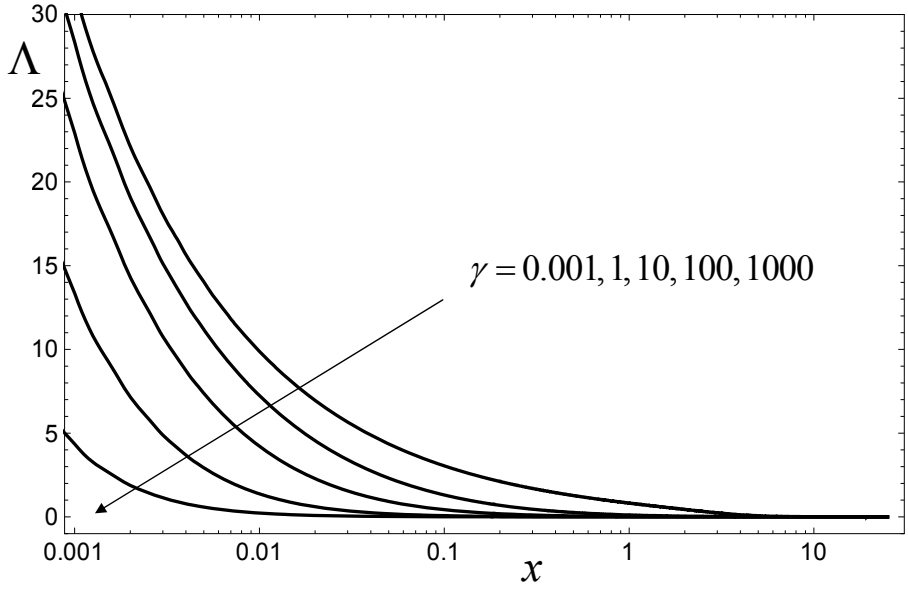

Figure 6: Behaviour of the parameter Λ as a function of x for different values of γ.

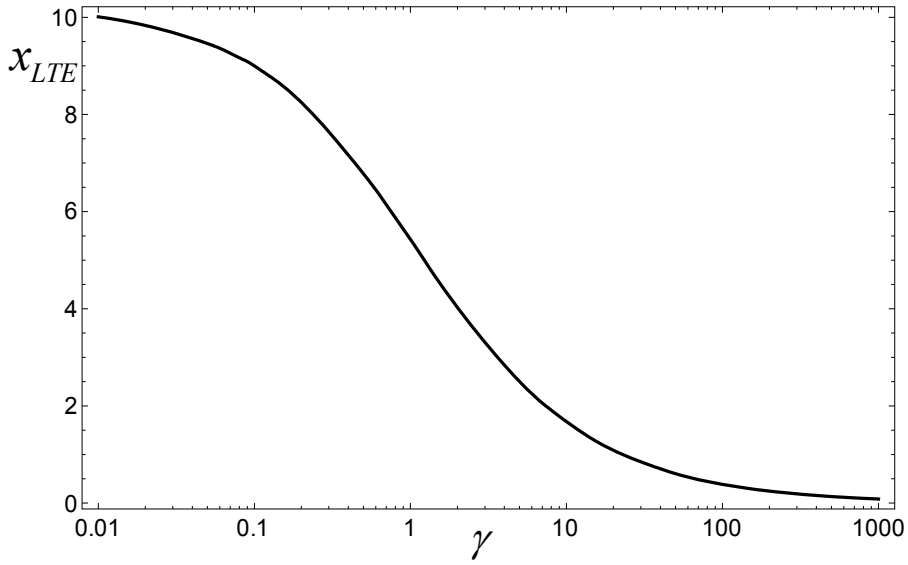

Figure 7: Variation with γ of the distance, x_{LTE}, at which local thermal equilibrium is attained.